ReToMe-VA: Recursive Token Merging for Video Diffusion-based Unrestricted Adversarial Attack

Anonymous Author(s)

ABSTRACT

Recent diffusion-based unrestricted attacks generate imperceptible adversarial examples with high transferability compared to previous unrestricted attacks and restricted attacks. However, existing works on diffusion-based unrestricted attacks are mostly focused on images yet are seldom explored in videos. In this paper, we propose the Recursive Token Merging for Video Diffusion-based Unrestricted Adversarial Attack (ReToMe-VA), which is the first framework to generate imperceptible adversarial video clips with higher transferability. Specifically, to achieve spatial imperceptibility, ReToMe-VA adopts a Timestep-wise Adversarial Latent Optimization (TALO) strategy that optimizes perturbations in diffusion models' latent space at each denoising step. TALO offers iterative and accurate updates to generate more powerful adversarial frames. TALO can further reduce memory consumption in gradient computation. Moreover, to achieve temporal imperceptibility, ReToMe-VA introduces a Recursive Token Merging (ReToMe) mechanism by matching and merging tokens across video frames in the self-attention module, resulting in temporally consistent adversarial videos. ReToMe concurrently facilitates inter-frame interactions into the attack process, inducing more diverse and robust gradients, thus leading to better adversarial transferability. Extensive experiments demonstrate the efficacy of ReToMe-VA, particularly in surpassing state-of-the-art attacks in adversarial transferability by more than 14.16% on average.

CCS CONCEPTS

• **Computing methodologies** → **Computer vision**.

KEYWORDS

action recognition, unrestricted adversarial attacks, diffusion models

1 INTRODUCTION

Recent years have witnessed remarkable performance exhibited by Deep Neural Networks (DNNs) across various computer vision and multimedia tasks [8, 13]. However, the emergence of adversarial examples has posed a challenge to the robustness of DNNs [11]. These adversarial examples, created by making imperceptible modifications to benign samples, can easily deceive state-of-the-art DNNs. Importantly, adversarial examples generated against one model can also mislead other models even with different architectures [6, 36]. The transferability of adversarial examples makes it feasible to carry out black-box attacks, which highlight security flaws in safety-critical scenarios, such as face verification [30] and surveillance video analysis [6], etc. To avoid potential risks, it is crucial to expose as many "blind spots" of DNNs by deeply exploring the transferability of adversarial examples.

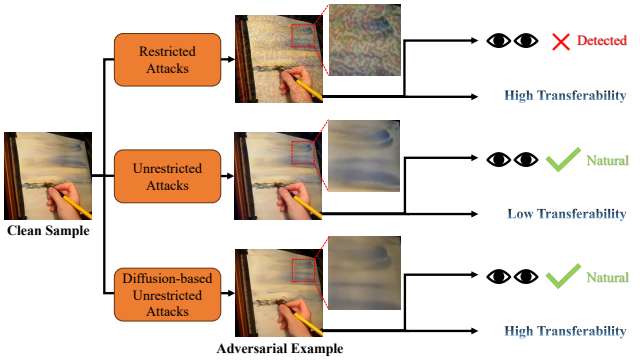

Figure 1: Difference between restricted attacks, unrestricted attacks, and diffusion-based unrestricted attacks.

Nowadays, the majority of transfer-based adversarial attacks [21, 38, 39] try to guarantee "subtle perturbation" by limiting the L_p-norm of the perturbation (a.k.a. restricted attacks). However, adversarial examples generated under L_p-norm constraint have human-perceptible perturbations, thereby rendering them more easily detectable [1, 46]. Therefore, unrestricted adversarial attacks [43, 45], which optimize unrestricted but natural changes (such as texture, style, color modifications, etc.) for given benign samples, are beginning to emerge. These unrestricted attacks yield more imperceptible perturbations but fall short in transferability compared to restricted attacks. With diffusion models drawing significant attention, recent works [5, 7] have employed diffusion models for unrestricted attacks to generate imperceptible adversarial examples with high transferability. The difference between previous unrestricted attacks, restricted attacks, and diffusion-based unrestricted attacks is displayed in Figure 1. Nevertheless, existing works on diffusion-based unrestricted attacks are mostly focused on images yet are seldom explored in videos.

This paper investigates transferable diffusion-based unrestricted attacks across different video recognition models. Specifically, we map each frame into the latent space and optimize the latents along the adversarial direction. The challenge of video diffusion-based unrestricted attacks comes from three aspects. Firstly, given the fact that diffusion models tend to add coarse semantic information in the early denoising steps [22], premature manipulation of the latents from previous work [7] yields significant alternations to the crafted frames compared to the corresponding benign frames.

MM '24, 28 October - 1 November 2024, Melbourne, Australia

ACM ISBN 978-1-4503-XXXX-X/18/06
https://doi.org/XXXXXXX.XXXXXXX

Concurrently, these spatial perceptible changes further result in temporal inconsistency in crafted adversarial videos when directly applying such generation to each frame. Consequently, further effort is needed to generate adversarial videos with temporal imperceptibility. Secondly, separately perturbing each benign frame induces monotonous gradients because the interactions among the video frames have not been fully exploited. Therefore, inter-frame interaction is necessary for boosting adversarial transferability. Lastly, the previous generation involves the gradient calculation throughout the entire denoising process, leading to a heavy memory overhead, especially when updating all the frames simultaneously.

To this end, we propose ReToMe-VA, which is the first video diffusion-based unrestricted adversarial attack framework, aiming at producing imperceptible adversarial video clips with higher transferability, as shown in Figure 2. Specifically, to achieve spatial imperceptibility, we introduce a Timestep-wise Adversarial Latent Optimization (TALO) that gradually updates perturbations in the latent space at each denoising timestep. Instead of calculating gradients of the entire denoising process, TALO only involves one timestep gradient calculation thereby reducing memory consumption in gradient computation. Furthermore, to reduce the spatial structure differences between benign and adversarial frames, TALO establishes constraints on the self-attention maps, which have been demonstrated to regulate structure effectively [5]. To effectively trade-off between spatial imperceptibility and adversarial transferability, TALO introduces the incremental iteration strategy, which prioritizes fewer iterations during the early timesteps to preserve the structure and increases the number of iterations during later timesteps to add more adversarial content. Therefore, TALO offers iterative and accurate updates to generate more powerful adversarial frames. To achieve temporal imperceptibility of adversarial video, we propose a novel Recursive Token Merging (ReToMe) mechanism, which recursively aligns tokens across frames according to the correlation and compresses the temporally redundant tokens to facilitate joint self-attention. With shared tokens in the self-attention module, ReToMe fixes the misalignment of details in per-frame optimization, resulting in temporally consistent adversarial videos. Additionally, inter-frame interaction can make the gradient of the current frame fuse information from associated frames, which has the potential to generate robust and diverse update directions to fool various target video models [34]. The ReToMe facilitates inter-frame interactions into the attack process, thus boosting the adversarial transferability.

Our contributions can be summarized as follows:

- We introduce the first framework for video diffusion-based unrestricted adversarial attacks, leveraging the Stable Diffusion model to generate imperceptible adversarial video clips with higher transferability.
- We propose a Timestep-wise Adversarial Latent Optimization strategy to achieve spatial imperceptibility. Besides, our novel recursive token merging mechanism maximally merges self-attention tokens across frames, thereby boosting adversarial transferability while achieving temporal imperceptibility.
- We conduct extensive experiments on video recognition models trained on both CNNs and Vits, as well as various defense methods. Our results demonstrate that ReToMe-VA surpasses the best baseline by an average of 14.16% and 17.32%, respectively.

2 RELATED WORK

As there are no previous works focusing on transferable video unrestricted attacks, this section reviews recent works on transferable unrestricted attacks against image models and transferable restricted attacks against video models.

2.1 Transferable Image Unrestricted Attacks

In the transferable image unrestricted attacks, color manipulation-based approaches play a significant role. Semantic Adversarial Examples (SAE) [15] converts the image from the RGB color space to the HSV color space, followed by random perturbation of both the H (Hue) and S (Saturation) channels. ReColorAdv [17] optimizes color transformation within the CIELUV color space, employing a flexibly parameterized function 'f' to recolor every pixel color 'c' to a new one. Colorization Attack (cAdv) [3] utilizes a pre-trained colorization network for color transformation, simultaneously adjusting input hints and masks to generate more natural adversarial examples. Unlike the previous one, Adversarial Color Enhancement (ACE) [45] generates adversarial images by using and optimizing a simple piece-wise linear differentiable color filter, with fewer parameters and better performance. To prevent human detection of unrestricted disturbances, ColorFool [29] manually selects four human-sensitive semantic classes and modifies colors within these sensitive regions constrainedly in the Lab color space. To make adversarial images more natural, Natural Color Fool (NCF) [43] constructs a "distribution of color distributions" for different semantic classes based on an existing dataset, using fused color distribution and optimizable transfer matrix to generate adversarial images.

Except for color manipulation-based methods, Texture Attack (tAdv) [3] fuses the texture of images from another class to generate adversarial examples, with an additional constraint on the victim image to prevent producing artistic images. Different from Texture Attack, Adversarial Content Attack (ACA) [7] introduces a diffusion model to perform unrestricted attacks on image models. By leveraging the diffusion model as a low-dimensional manifold, ACA maps the victim image into the latent space, where adversarial attacks and optimizations are conducted. When compared to both color manipulation-based methods and texture attacks, ACA demonstrates superior capability in generating natural adversarial image examples by harnessing the powerful generative capacity of diffusion models. Therefore, this paper investigates the potential of leveraging the diffusion model to perform transferable video unrestricted attacks.

2.2 Transferable Video Restricted Attacks

In the transferable video restricted attacks, Temporal Translation (TT) [37] is a representative method, which prevents overfitting the surrogate model by optimizing adversarial perturbations over a set of temporal translated video clips, to enhance the transferability of video adversarial examples across different video models. Most recently, based on the observation that the intermediate features between image models and video models are somewhat similar [38],

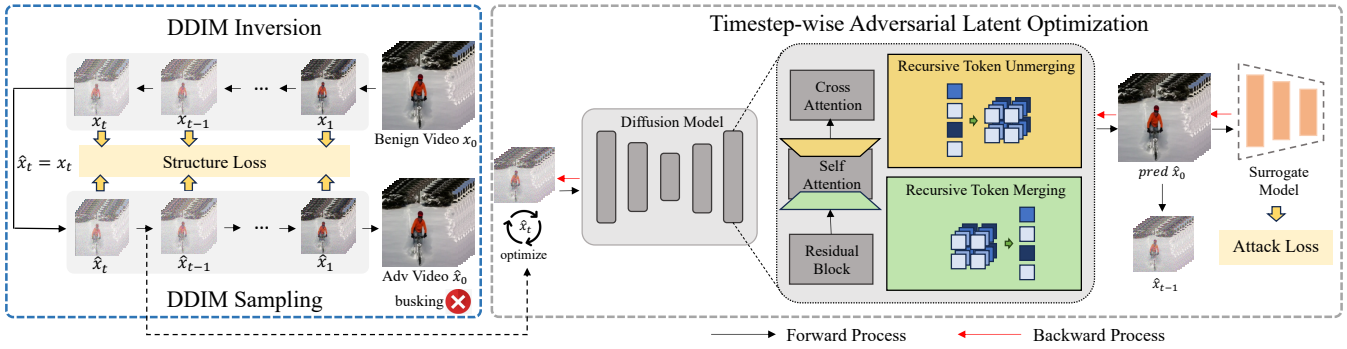

Figure 2: Framework overview of the proposed ReToMe-VA. For a video clip, DDIM inversion is applied to map the benign frames into the latent space. Timestep-wise Adversarial Latent Optimization is employed during the DDIM sampling process to optimize the latents. Throughout the whole pipeline, Recursive Token Merging and Recursive Token Unmerging Modules are integrated into the diffusion model to enhance its effectiveness. Additionally, structure loss is utilized to maintain the structural consistency of video frames. Ultimately, the resulting adversarial video clip is capable of deceiving the target model.

some transferable cross-modal attacks from images to videos have emerged. For instance, Image To Video (I2V) [38] generates adversarial video clips on the ImageNet pre-trained model by minimizing the cosine similarity between intermediate features of each benign frame and its adversarial frame. However, I2V treats a video clip as an orderless image set and ignores the inherent temporal information in video clips. In contrast, Global-Local Characteristic Excited Cross-Modal Attack [34] fully considers video characteristics from both global and local perspectives, which performs global inter-frame interactions in the attack process to induce more diverse and stronger gradients and proposes local correlation disturbance to prevent the target video model from capturing valid temporal clues. Furthermore, Generative Cross-Modal Attack (GCMA) [6] trains perturbation generators against the ImageNet domain but can fool target models from video domains, which proposes a random motion module and a temporal consistency loss based on intermediate features to narrow the gap between the image and video domains. Different from all of the prevision works that focus on restricted attacks, this work studies unrestricted attacks on video models.

3 METHODOLOGY

3.1 Diffusion-based Unrestricted Attack Framework

Given a benign video clip $x \in \mathcal{X} \subset \mathbb{R}^{N\times H\times W\times C}$ with N frames $\{x^1, x^2, ..., x^N\}$ and its corresponding ground-truth label $y \in \mathcal{Y} = \{1, 2, ...K\}$, where N, H, W, C denote the number of frames, height, width and the number of channels respectively, K denotes the number of classes. Let F_θ denote the video recognition model trained on the video dataset $\mathcal{X}$. We use $F_\theta(x) : \mathcal{X} \rightarrow \mathcal{Y}$ to denote the prediction of the video recognition model $F_\theta(x)$ for x. Our goal is to craft unrestricted adversarial video clip $\hat{x}$ against a surrogate video recognition model $G\phi$ leveraging the Stable Diffusion [28] to deceive the target video recognition model F_θ.

Prior works on image diffusion-based unrestricted attacks [5, 7] use the DDIM inversion [23] technology to map the benign image back into the diffusion latent space by reversing the deterministic sampling process, then optimize the latent of the image along the adversarial direction. Finally, the adversarial image is generated from the optimized adversarial latent through the entire denoising process. For simplicity, the encoding and decoding of the VAE is ignored, as it is differentiable. However, such generation has obvious limitations for video attacks when applied directly to each frame. Firstly, given the fact that diffusion models tend to add coarse semantic information during the early denoising steps [22], premature manipulation tends to change the layouts or semantic structure of frames, which leads to semantic inconsistency and changes. This spatial inconsistency further leads to temporal inconsistency in adversarial videos. Furthermore, because this framework applied in video attacks involves updating all the frames simultaneously, the gradient calculation throughout the entire denoising process leads to a heavy memory overhead and large time consumption.

Therefore, we propose our ReToMe-VA to address these challenges, as shown in Figure 2. Specifically, we utilize the Timestep-wise Adversarial Latent Optimization (Sec.3.2) in the denoising process and introduce a Recursive Token Merging (Sec.3.3) technique to maintain the temporal consistency and boost adversarial transferability. The algorithm of ReToMe-VA is presented in Algorithm 1.

3.2 Timestep-wise Adversarial Latent Optimization

Existing latent optimization approaches which update latent at a fixed timestep are usually insufficiently flexible and stable in controlling the generation of adversarial video clips, therefore we propose Timestep-wise Adversarial Latent Optimization (TALO) to gradually update perturbations in the latent space at each denoising timestep. After the inversion of the DDIM, we obtain the reversed latents $\{x_0, x_1, ..., x_T\}$ from timestep 0 to T, where x_0 is x. For the trade-off between imperceptibility and adversarial transferability, we start adversarial optimization from the latent x_{t_s} at t_s timestep rather than from Gaussian noise at T timestep. We denote $\hat{x}_t$ as the adversarial latents at t timestep, we initialize $\hat{x}_{t_s} = x_{t_s}$. At each timestep t of denoising, we predict the final output $\hat{x}_0^t$ for each

frame to substitute the adversarial output $\hat{x}_0$ for the prediction of the surrogate model G_ϕ. The calculation of $\hat{x}_0^t$ and our adversarial objective function is expressed as follows:

$$\hat{x}_0^t = \frac{\hat{x}_t - \sqrt{1-\alpha_t}\epsilon_\theta(\hat{x}_t, t)}{\sqrt{\alpha_t}} \tag{1}$$

$$\arg\min_{\hat{x}_t} \mathcal{L}_{attack} = -J(\hat{x}_0^t, y, G\phi) \tag{2}$$

where α_t represents the parameters of the scheduler, ϵ_θ denotes the noise predicted by the UNet, and $J(\cdot)$ is the cross-entropy loss. After optimizing latents $\hat{x}_t$, we generate a sample $\hat{x}_{t-1}$ from $\hat{x}_t$ for the preparation of next timestep-wise optimization via:

$$\hat{x}_{t-1} = \sqrt{\alpha_{t-1}}\left(\frac{\hat{x}_t - \sqrt{1-\alpha_t}\epsilon_\theta(\hat{x}_t, t)}{\sqrt{\alpha_t}}\right) + \sqrt{1-\alpha_{t-1}-\sigma_t^2}\epsilon_\theta(\hat{x}_t, t) \tag{3}$$

Finally, $\hat{x}_0$ is used as the final adversarial video clip $\hat{x}$ to fool the target video recognition model F_θ.

Preservation of Structural Similarity. Adversarial optimization at each denoising step leads to a deviation of the latent from the original frame distribution. Despite the inevitable alterations to the benign frames for adding adversarial content, the challenge lies in preserving the structural similarity of the adversarial frames from the benign frames. Leveraging the fact that the spatial features of the self-attention layers are influential in determining both the structure and the appearance of the generated images, TALO minimizes the average difference of the self-attention maps between the benign and the adversarial latent at each timestep t:

$$\arg\min_{\hat{x}_t} \mathcal{L}_{structure} = \sum_{j \in n_s} ||\hat{s}_t^j - s_t^j||_2^2 \tag{4}$$

where s_t^j, $\hat{s}_t^j$ are respectively the j-th self-attention map of benign latents x_t and adversarial latents $\hat{x}_t$, n_s denotes the total number of self-attention maps in the diffusion model.

In general, the final objective function of ReToMe-VA is as follows, where γ and β represent the weight factors of each loss:

$$\arg\min_{\hat{x}_t} \mathcal{L}_{total} = \gamma\mathcal{L}_{attack} + \beta\mathcal{L}_{structure} \tag{5}$$

Incremental Iteration Strategy. TALO iteratively optimizes $\hat{x}_t$ to seek optimal adversarial latents at timestep t and the iteration number represents a trade-off between spatial imperceptibility and adversarial transferability. Recent work [22] has indicated that the diffusion models tend to add coarse semantic information (e.g., layout) during the early timesteps while more fine details during the later timesteps. As depicted in Table 6, a smaller number of iterations fail to find better perturbations, reducing the low adversarial transferability. Conversely, a larger number of iterations render adversarial frames deviating more from the benign frames, adversely affecting the spatial imperceptibility of the adversarial video clip. Therefore, we adopt an Incremental Iteration (II) strategy, starting with fewer attack iterations during the early timesteps to preserve structure and gradually increasing the number of iterations during the later timesteps to add adversarial details.

Our TALO strategy has two advantages. First, timestep-wise optimization with II strategy provides a more controllable and stable process during adversarial generation making more powerful adversarial video clips with spatial imperceptibility. Second, TALO only involves one timestep gradient computation thereby reducing memory consumption in gradient computation.

Algorithm 1: Framework of ReToMe-VA

Input: a benign video clip x with label y, a surrogate classifier G_ϕ, DDIM steps T, start attack DDIM timestep t_s, initial attack iteration N_a, recursive token merging ratio p, weight factors γ, β.
Output: Unrestricted adversarial video clip $\hat{x}$.

```
Add Recursive Token Merging and Recursive Token Unmerging Module to Stable Diffusion;
Calculate latents {x_1, ..., x_{t_s}} using DDIM inversion;
x̂_{t_s} ← x_{t_s};
for t ← t_s to 1 do
    for j ← 1 to N_a + 2(t_s − t) do
        x̂_0^t = (x̂_t − √(1−α_t) ε_θ(x̂_t, t)) / √α_t;
        Calculate the attack loss L_attack as Eq. 2;
        Calculate the structure loss L_structure as Eq. 4;
        Update x̂_t over total loss L_total Eq. 5 with AdamW optimizer;
        x̂_{t−1} ← Eq. 3 ;
x̂ ← x̂_0;
return x̂
```

3.3 Recursive Token Merging

TALO strategy perturbs each benign frame of video separately. This per-frame optimization makes the frames likely optimized along different adversarial directions resulting in motion discontinuity and temporal inconsistency. Furthermore, separately perturbing each benign frame reduces the monotonous gradients because the interactions among the frames are not exploited. To this end, we introduce a recursive token merging (ReToMe) strategy that recursively matches and merges similar tokens across frames together enabling the self-attention module to extract consistent features. In the following, we first provide the basic operation of token merging and token unmerging and then our recursive token merging algorithm.

Generally, tokens T are partitioned into a source (src) and destination (dst) set. Then, tokens in src are matched to their most similar token in dst, and r most similar edges are selected subsequently. Next, we merge the connected r most similar tokens in src to dst by replacing them as the linked dst tokens. To keep the token number unchanged, we divide merged tokens after self-attention by assigning their values to merged tokens in src. Token matching, merging, and unmerging operations are expressed as:

$$\begin{aligned} e &= match(src, dst, r), \\ T_m &= M(T, e), T_{um} = UM(T_m, e). \end{aligned} \tag{6}$$

where $match(\cdot)$ outputs the matching map e with r edges from src to dst, $M(\cdot)$ and $UM(\cdot)$ merge and unmerge tokens according to matching e. After token merging operation, $T_m = \{(T^{src})^{um}, T^{dst}\}$ consists the unmerged tokens $(T^{src})^{um}$ in src and tokens T^{dst} in

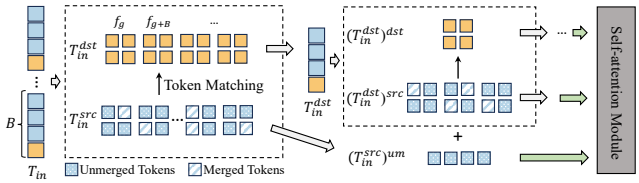

Figure 3: Recursive token merging process.

dst, while merged tokens $(T^{src})^m$ in src is replaced by tokens in dst.

A self-attention module takes a sequence of input and output tokens across all frames. The input and output tokens are denoted as $T_{in}, T_{out} \subset \mathbb{R}^{N\times L\times E}$, where L is the number of tokens per frame, and E is the embedding dimension. To partition tokens across frames into src and dst, we define stride as B, we randomly choose one out of the first B frames (e.g. the g^{th} frame), and select the subsequent frames every B interval into the dst set (named as T_{in}^{dst}). Tokens of other frames are in src set (T_{in}^{src}). Then merging operation mentioned above in Eq. 6 is used to merge source frames:

$$\begin{aligned} e_1 &= match(T_{in}^{src}, T_{in}^{dst}, r_1), \\ T_{rm} &= M(T_{in}, e1). \end{aligned} \tag{7}$$

where $T_{rm} = \{T_{in}^{dst}, (T_{in}^{src})^{um}\}$. We set $r_1 = p(N - N_{d_1})L$ where p is the merging ratio, $(N - N_{d_1})L$ is the src token number in the first merging process and N_{d_1} is the T_{in}^{dst} frame number.

Nevertheless, during the merging process expressed above, tokens in dst are not merged and compressed. To maximally fuse the inter-frame information, we recursively apply the above merging process to tokens in dst until they contain only one frame. For instance, in the next merging process of T_{in}^{dst}, after partition of src and dst of T_{in}^{dst} (named as $(T_{in}^{dst})^{src}$ and $(T_{in}^{dst})^{dst}$), we merge tokens in src to dst by:

$$\begin{aligned} e_2 &= match((T_{in}^{dst})^{src}, (T_{in}^{dst})^{dst} + (T_{in}^{src})^{um}, r_2), \\ (T_{in}^{dst})_{rm} &= M(T_{in}^{dst}, e_2). \end{aligned} \tag{8}$$

We set $r_2 = p(N_{d_1} - N_{d_2})L$ where $(N_{d_1} - N_{d_2})L$ is the src token number and N_{d_2} is dst frame number in this process. The difference is that we add the previous unmerged tokens $(T_{in}^{src})^{um}$ into dst for token matching. Then we replace T_{in}^{dst} with $(T_{in}^{dst})_{rm}$ in T_{rm}. The token merging process of ReToMe is shown in Figure 3. Next, we input the tokens T_{rm} into the self-attention module to calculate $(T_{out})_{rm}$.

The output tokens $(T_{out})_{rm}$ need to be restored to their original shape T_{out} to perform the following operations. Therefore, in the unmerge process, the unmerging operation in Eq. 6 is applied in the reverse order of the merging process to get T_{out}.

Our ReToMe has three advantages. Firstly, ReToMe ensures that the most similar tokens share identical outputs, maximizing the compression of tokens. This approach fosters internal uniformity of features across frames and preserves temporal consistency, thereby effectively achieving temporal imperceptibility. Secondly, given the fact that there is a negative correlation between the adversarial transferability and the interaction inside adversarial perturbations [35], the merged tokens decrease interaction inside adversarial perturbations, effectively preventing overfitting on the surrogate model. Furthermore, the tokens in dst linked to merged tokens facilitate inter-frame interaction in gradient calculation, which may induce more robust and diverse gradients [34]. Therefore, ReToMe can effectively boost adversarial transferability.

4 EXPERIMENT

4.1 Experiment Settings

Dataset. We evaluate the adversarial transferability of our proposed method on Kinetics-400 [4] dataset. The dataset contains approximately 240,000 videos from 400 human action classes, we carefully selected one video clip from each class that was correctly classified by all video recognition models, yielding a total of 400 videos as the validation dataset.

Models. To assess the adversarial robustness of network architectures, we select CNNs and ViTs as the attacked models, respectively. For CNNs, we choose normally trained I3D SLOW [9], TPN [42] with two different backbones: ResNet-50 and ResNet-101, and R(2+1)D [33] with backbone ResNet-50 (R(2+1)D-50). For ViTs, we consider VTN [24], Motionformer [2], TimeSformer [26], Video Swin [19].

Implementation Details. Our experiments are run on an NVIDIA A800 with Pytorch. We set DDIM steps $T = 20$, start attack DDIM step $t_s = 5$, initial attack Iteration $N_a = 4$, recursive token merging ratio $p = 0.5$. Meanwhile, the weight factors γ, β in Eq. 5 are set to 10, 100 respectively. We adopt AdamW [20] with the learning rate set to $1e^{-2}$. The version of Stable Diffusion we used is v2.0.

Evaluation Metrics. We use the Attack Success Rate (ASR), i.e., the percentage of adversarial video clips that are successfully misclassified by the video recognition model, to evaluate the adversarial transferability. Thus a higher ASR means better adversarial transferability. If not specifically stated, Avg.ASR is the average ASR over all target video models. Besides, we quantitatively assess the frame quality using two reference perceptual image quality measures including Frechet Inception Distance (FID) [14] and LPIPS [44], and three non-reference perceptual image quality measures NIMA-AVA [32], HyperIQA [31], and TReS [10]. For temporal consistency, we adopt four evaluation metrics in VBench [16], including Subject Consistency, Background Consistency, Motion Smoothness, and Temporal Flickering. Each metric is tailored to specific aspects of video analysis. Subject Consistency measures whether an object's appearance remains consistent throughout the video. Background Consistency evaluates the temporal uniformity of background scenes through CLIP [27] feature similarity across frames. Motion Smoothness assesses the smoothness and realism of motion, adhering to real-world physics. Temporal Flickering computes the mean absolute difference across frames to detect abrupt changes. Moreover, we also select Pixel-MSE to evaluate the naturalness and continuity of frame-to-frame transitions. Specifically, each frame in the adversarial video clip is warped to the next frame by the optical flow between consecutive frames. Then, we compute the average mean-squared pixel error between each warped frame and its corresponding next frame.

Table 1: Performance comparison of adversarial transferability on normally trained CNNs and ViTs. We report attack success rates (%) of each method ("*" is white-box attack results). The best results are highlighted in bold.

Surrogate Model	Attack	Models									Avg. ASR (%)
		CNNs					Transformers				
		Slow-50	Slow-101	TPN-50	TPN-101	R(2+1)D-50	VTN	Motionformer	TimeSformer	Video Swin	
Slow-50	TT	99.00*	74.00	**96.50**	72.00	66.25	5.50	3.50	6.75	10.75	41.91
	SAE	37.75*	9.00	12.75	8.50	60.50	14.00	22.25	37.75	21.25	20.41
	ReColorAdv	**100.00***	64.50	96.25	56.25	68.00	7.25	4.75	13.25	11.75	40.25
	cAdv	98.75*	29.00	43.25	30.00	28.25	25.00	21.50	**44.25**	24.25	30.69
	tAdv	99.50*	7.00	13.25	7.50	36.00	4.50	2.75	9.25	6.25	10.81
	ACE	89.25*	3.75	6.50	4.25	24.00	3.25	4.00	9.75	4.75	7.53
	ColorFool	31.75*	5.25	9.50	7.50	50.25	11.50	19.25	30.75	17.50	16.62
	NCF	37.25*	12.25	21.25	10.50	54.00	12.00	15.50	25.00	13.25	18.38
	ACA	67.75*	38.50	47.75	36.00	**68.75**	25.00	22.50	32.75	28.25	37.44
	Ours	96.50*	**78.50**	89.50	**77.00**	61.25	**30.25**	**25.25**	39.50	**35.50**	**54.59**
TPN-50	TT	92.00	52.50	**100.00***	53.25	63.50	4.75	2.25	8.25	8.25	35.59
	SAE	9.00	7.00	36.25*	6.50	59.00	14.50	21.50	40.25	21.50	19.56
	ReColorAdv	67.00	27.25	**100.00***	27.75	56.75	3.50	2.25	8.25	5.50	24.78
	cAdv	31.50	18.75	98.25*	21.50	28.75	22.00	17.75	39.50	19.25	24.88
	tAdv	12.25	7.00	98.00*	6.50	33.50	6.25	3.00	9.00	6.25	10.47
	ACE	4.00	3.50	86.75*	2.75	22.00	4.25	3.75	10.50	4.75	6.94
	ColorFool	8.75	6.00	35.00*	5.75	45.50	8.75	17.50	28.50	14.50	15.59
	NCF	20.25	10.25	32.00*	9.75	53.75	10.75	14.75	26.50	12.25	17.06
	ACA	43.75	33.25	63.75*	33.50	**67.00**	**24.00**	**22.75**	32.75	27.50	35.56
	Ours	**80.50**	**58.75**	97.50*	**61.75**	52.75	20.75	19.75	**33.00**	**27.25**	**44.31**
VTN	TT	11.25	10.00	10.50	5.50	56.00	**100.00***	64.50	83.50	14.25	31.94
	SAE	8.75	6.25	9.00	7.25	55.00	48.75*	19.00	39.75	22.50	20.16
	ReColorAdv	4.50	4.50	5.75	4.25	42.50	**100.00***	43.75	62.00	10.50	22.22
	cAdv	16.25	14.50	16.50	17.25	28.00	99.75*	38.50	67.25	27.00	16.28
	tAdv	7.25	6.00	7.75	5.25	32.25	94.00*	14.75	28.50	9.75	13.94
	ACE	3.00	2.00	3.00	2.00	22.75	71.25*	5.50	18.50	3.50	7.53
	ColorFool	5.75	5.25	9.00	5.50	40.00	41.50*	18.50	30.75	15.50	19.08
	NCF	16.50	10.75	15.75	9.75	53.75	72.25*	24.75	39.25	14.00	21.66
	ACA	**28.75**	**28.00**	**28.75**	**25.50**	**66.75**	59.50*	32.00	42.00	28.75	35.06
	Ours	27.25	25.25	28.25	23.00	49.00	99.25*	**75.50**	**88.25**	**43.25**	**44.97**
Motionformer	TT	12.75	12.50	11.00	8.00	57.75	91.75	**100.00***	86.50	29.50	38.72
	SAE	7.75	4.50	6.75	4.25	49.50	11.50	72.00*	31.75	14.00	16.25
	ReColorAdv	2.50	1.50	3.25	2.00	36.00	15.50	**100.00***	25.50	2.00	11.03
	cAdv	9.00	7.25	9.00	9.00	21.00	25.00	89.25*	48.50	12.25	17.62
	tAdv	12.75	12.00	13.00	12.00	38.00	12.25	51.50*	20.75	11.50	16.53
	ACE	1.75	1.75	2.25	0.25	6.00	0.75	50.00*	6.50	2.25	2.69
	ColorFool	3.50	2.75	5.50	4.50	33.00	5.00	71.50*	26.00	8.00	11.03
	NCF	12.50	9.25	15.00	7.50	53.25	12.75	*39.75	30.25	12.50	17.44
	ACA	27.00	27.50	25.75	24.50	**65.75**	31.50	67.75*	37.75	24.50	33.03
	Ours	**42.50**	**44.25**	**44.25**	**42.75**	57.50	**91.25**	**100.00***	**91.00**	**63.75**	**59.66**
TimeSformer	TT	10.75	10.00	10.25	6.25	57.00	**85.25**	57.25	**100.00***	16.00	31.59
	SAE	5.00	3.75	4.75	3.50	43.75	8.00	14.75	72.50*	14.75	12.28
	ReColorAdv	7.50	6.75	7.00	5.25	49.25	59.00	38.50	**100.00***	10.00	22.91
	cAdv	10.50	11.25	12.00	10.00	23.25	43.25	31.00	**100.00***	24.25	20.69
	tAdv	5.50	5.00	5.50	4.50	30.50	17.00	10.25	95.00*	7.00	10.66
	ACE	3.00	2.75	3.75	1.00	18.00	4.50	3.25	89.75*	3.50	4.97
	ColorFool	5.25	3.00	5.00	2.75	33.25	5.00	8.50	65.75*	8.50	8.91
	NCF	16.50	10.00	17.00	9.75	53.00	21.50	27.75	92.75*	17.75	29.56
	ACA	**30.75**	28.25	29.50	27.00	**67.00**	46.00	36.00	72.25*	30.25	36.84
	Ours	28.00	**29.50**	**32.00**	**28.50**	49.75	85.00	**76.50**	**100.00***	**47.00**	**47.03**

4.2 Attacks against Normally Trained Models

We first assess the adversarial transferability of normally trained CNNs and ViTs. For video restricted attacks, we compare the proposed method with state-of-the-art TT [37]. For video unrestricted attacks, due to the lack of comparable work, we extend the image unrestricted attacks to generate adversarial video clips frame-by-frame, including SAE [15], ReColorAdv [17], cAdv [3], tAdv [3], ACE [45], ColorFool [29], NCF [43], and ACA [7]. Adversarial video clips are crafted against Slow-50, TPN-50, VTN, Motionformer and TimeSformer respectively. The transferability of different methods is displayed in Table 1.

It can be observed that adversarial video clips generated by ReToMe-VA generally exhibit superior transferability compared to those generated by state-of-the-art competitors. Our proposed ReToMe-VA achieved a white-box attack success rate of 100% on the Motionformer and TimeSformer models. The results from Table 1 indicate that our method surpasses the restricted attack method TT in the black-box setting. When Slow-50, Motionformer, and TimeSformer are used as surrogate models, we significantly outperform state-of-the-art ACA by 17.10%, 26.62%, and 10.19%, respectively, indicating that our ReToMe-VA has higher transferability under the more challenging cross-architecture setting. Specifically, when the surrogate model is Slow-50, we surpass ACA by significant margins of 40%, 41.75%,41%, and 6.75% in Slow-101, TPN-50, TPN-101, and TimeSformer, respectively.

4.3 Attacks against Adversarial Defense Mechanisms

We also assess its performance against five representative defense mechanisms, including the top-2 defense methods in the NIPS 2017 competition (high-level representation guided denoiser (HGD) [18] and random resizing and padding (R&P) [40]), three popular input

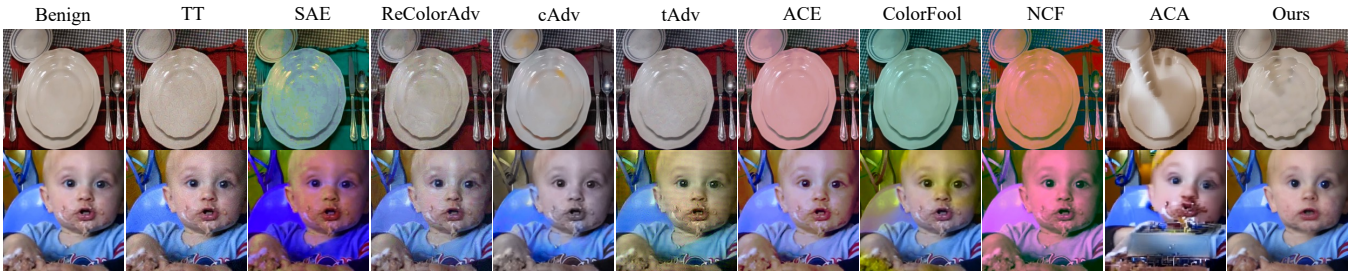

(a) Visualization of state-of-the-art attacks

(b) Adversarial frames of ReToMe-VA

Figure 4: Qualitative results of frame quality. (a) Visual quality comparisons among different attack methods. (b) More adversarial frames generated from ReToMe-VA. The Left is the benign frame and the right is the adversarial frame.

Table 2: Robustness on adversarial defense methods. We report Avg.ASR(%) of each method. The best results are in bold.

Attack Method	HGD	R&P	JPEG	Bit-Red	DiffPure
TT	37.69	29.47	31.69	38.56	12.59
SAE	24.03	25.00	26.34	27.81	37.31
ReColorAdv	35.81	29.13	29.84	35.53	15.69
cAdv	31.31	30.19	32.00	34.03	38.09
tAdv	10.00	10.63	11.28	15.34	15.72
ACE	8.09	9.31	10.40	12.84	20.71
ColorFool	18.88	20.50	21.25	22.94	33.56
NCF	20.69	22.25	21.69	24.75	32.16
ACA	35.90	28.22	29.84	35.53	36.56
Ours	**53.41**	**50.97**	**52.72**	**54.56**	**40.97**

pre-process defenses, namely jpeg compression (JPEG) [12], bit depth reduction (Bit-Red) [41], and DiffPure [25]. We take Slow-50 as a surrogate model and all of the adversarial video clips are crafted on it.

From the results demonstrated in Table 2, we can see our method displays superiority over other advanced attacks by a significant margin. For example, against HGD and DiffPure defenses, our method outperforms the next best attack ACA by over 17.5% and 4.41% respectively, indicating its robustness and efficiency in penetrating these defenses. This evidences the advanced capability of our method in maintaining high attack success rates under diverse adversarial defense methods.

4.4 Visualization

In this section, we will demonstrate the superiority of our approach through qualitative and quantitative comparisons of frame quality and temporal consistency in videos.

Frame Quality. In Figure 4(a), we visualize the adversarial frames crafted by different attack approaches. We can see that our attack

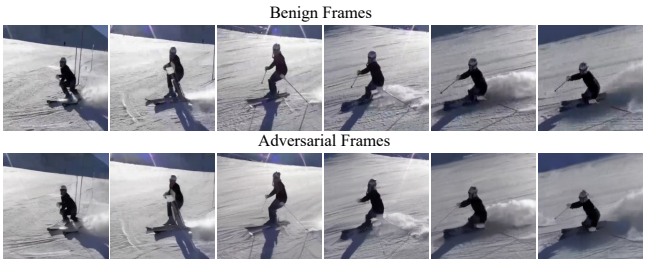

Figure 5: A Sample of generated video from our method.

is much more natural than the restricted attack TT and more imperceptible compared with other unrestricted attacks. In detail, the color and texture changes of adversarial frames generated by SAE, ACE, ColorFool, NCF, and ACA are easily perceptible. Next, we give more adversarial frames generated by ReToMe-VA in Figure 4(b). It is observed that our method adaptively modifies inconspicuous details to generate adversarial frames. For example, minor alteration is made to the texture of the knitted yarn in the frame in the fourth column of Figure 4(b). Moreover, we quantitatively assess the frame quality using the reference and non-reference perceptual image quality measures. As illustrated in Table 4, our method achieves top-2 performance across all metrics. And ReToMe-VA achieves the best result in HyperIQA and TReS.

Temporal Consistency. To provide a qualitative comparison, Figure 5 shows an adversarial video clip crafted by our ReToMe-VA. From the visualization of the video, we can observe that our proposed method produces high-quality frames. The crafted frames by ReToMe-Va highly align with the benign frames in both appearance and structure and also maintain a high level of motion consistency with the benign frames. Quantitative evaluation results are shown in Table 3, we evaluate the temporal quality of the videos using five metrics, all of which achieve top-2 results. Specifically, Motion

Table 3: Quantitative comparison of temporal consistency. The best results are in bold and the second-best results are underlined.

Attack Method	Subject Consistency↑	Background Consistency↑	Motion Smoothness↑	Temporal Flickering↑	Pixel-MSE↓
SAE	79.23%	87.08%	82.61%	80.61%	94.17
ReColorAdv	87.69%	91.72%	95.07%	93.00%	69.99
cAdv	86.43%	90.62%	94.28%	92.31%	67.56
tAdv	**88.81%**	**93.29%**	95.50%	93.44%	**57.50**
ACE	85.03%	91.83%	92.27%	90.19%	85.01
ColorFool	78.94%	88.29%	79.44%	76.88%	83.81
NCF	79.82%	89.37%	87.65%	85.02%	95.58
ACA	75.67%	85.89%	94.10%	91.96%	68.98
Ours	88.03%	92.21%	**95.62%**	**93.76%**	58.66

Smoothness and Temporal Flickering yield the best results. Therefore, our method demonstrates superior performance in terms of video temporal consistency.

Table 4: Quantitative evaluation of image quality. The best results are highlighted in bold while the second-best results are underlined. NA denotes Not Applicable.

Attack Method	FID↓	LPIPS↓	NIMA-AVA↑	HyperIQA↑	TReS↑
Benign	NA	NA	5.38	50.97	59.80
TT	43.15	0.13	5.46	50.81	58.08
SAE	57.66	0.39	**5.64**	49.61	57.22
ReColorAdv	50.40	0.13	5.46	50.81	58.08
cAdv	47.02	0.20	5.61	52.58	61.41
tAdv	36.75	**0.08**	5.37	49.46	57.30
ACE	**21.63**	0.13	5.31	51.28	59.92
ColorFool	48.79	0.38	5.18	50.13	58.98
NCF	37.02	0.32	5.18	48.95	54.95
ACA	41.69	0.24	5.60	48.74	55.86
Ours	25.63	0.10	5.62	**55.53**	**66.31**

4.5 Ablation Studies

In Table 5, we ablate the designs mentioned in Section 3.3. We can observe that the avg.ASR and Subject Consistency increase by 6.08% and 0.04 by using ReToMe, indicating that the Recursive Token Merging Technique exhibits strong adversarial transferability and enhanced temporal consistency. Additionally, the ablation study of II strategy is shown in Table 6. In detail, the first two lines denote that we fix the iteration number at each timestep, while the last line displays our II strategy. The results verify that our II strategy performs a good trade-off between transferability and spatial imperceptibility.

ReToMe	Avg.ASR	Subject Consistency
w/o	53.17	0.8410
w/	59.25	0.8803

Table 5: Ablation study of ReToMe.

Iter Strategy	Avg. ASR (%)	FID
Fix Iter 4	44.69	18.86
Fix Iter 12	70.11	33.42
Iter 4→12	59.25	25.63

Table 6: Ablation study of II strategy.

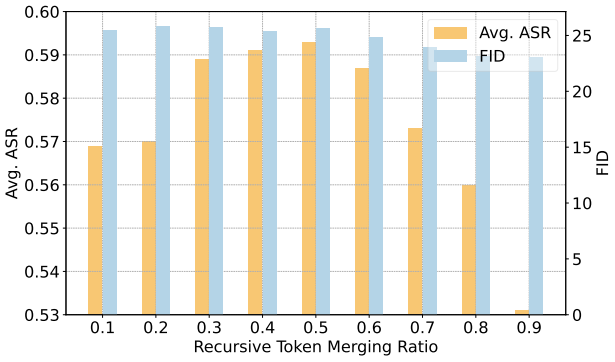

Figure 6: Comparison of different merging ratios.

Moreover, we investigate the impact of different merging ratios on adversarial transferability and video quality, using Slow-50 as an example surrogate model. The results are illustrated in Figure 6, which demonstrate that a merging ratio of $p = 0.5$ achieves the best adversarial transferability with high frame quality.

5 CONCLUSION

In this paper, we propose the Recursive Token Merging for Video Diffusion-based Unrestricted Adversarial Attack (ReToMe-VA). As far as we know, this is the first diffusion-based framework to generate imperceptible adversarial video clips with higher transferability. ReToMe-VA adopts a Timestep-wise Adversarial Latent Optimization strategy to achieve spatial imperceptibility. Moreover, ReToMe-VA introduces a Recursive Token Merging (ReToMe) mechanism. By aligning and compressing redundant tokens across frames, ReToMe produces temporally consistent adversarial videos. ReToMe provides more diverse and robust attack direction by incorporating inter-frame interactions into the adversarial optimization process, consequently boosting adversarial transferability. Extensive experiments and visualization demonstrate the efficacy of ReToMe-VA, particularly in surpassing the best baseline by an average of 14.16% in normally trained models. We hope our work will pave the way for future research in enhancing the robustness of video recognition models against adversarial threats, as well as contributing to the development of more effective video adversarial attack methods.

REFERENCES

[1] Jonathan Aigrain and Marcin Detyniecki. 2019. Detecting adversarial examples and other misclassifications in neural networks by introspection. *arXiv preprint arXiv:1905.09186* (2019).

[2] Gedas Bertasius, Heng Wang, and Lorenzo Torresani. 2021. Is space-time attention all you need for video understanding?. In *ICML*, Vol. 2. 4.

[3] Anand Bhattad, Min Jin Chong, Kaizhao Liang, Bo Li, and D. A. Forsyth. 2020. Unrestricted Adversarial Examples via Semantic Manipulation. In *International Conference on Learning Representations*. https://openreview.net/forum?id=Sye_OgHFwH

[4] Joao Carreira and Andrew Zisserman. 2017. Quo vadis, action recognition? a new model and the kinetics dataset. In *proceedings of the IEEE Conference on Computer Vision and Pattern Recognition*. 6299–6308.

[5] Jianqi Chen, Hao Chen, Keyan Chen, Yilan Zhang, Zhengxia Zou, and Zhenwei Shi. 2023. Diffusion models for imperceptible and transferable adversarial attack. *arXiv preprint arXiv:2305.08192* (2023).

[6] Kai Chen, Zhipeng Wei, Jingjing Chen, Zuxuan Wu, and Yu-Gang Jiang. 2023. GCMA: Generative Cross-Modal Transferable Adversarial Attacks from Images to Videos. In *Proceedings of the 31st ACM International Conference on Multimedia*. 698–708.

[7] Zhaoyu Chen, Bo Li, Shuang Wu, Kaixun Jiang, Shouhong Ding, and Wenqiang Zhang. 2023. Content-based Unrestricted Adversarial Attack. In *Advances in Neural Information Processing Systems*, A. Oh, T. Neumann, A. Globerson, K. Saenko, M. Hardt, and S. Levine (Eds.), Vol. 36. Curran Associates, Inc., 51719–51733. https://proceedings.neurips.cc/paper_files/paper/2023/file/a24cd16bc361afa78e57d31d34f3d936-Paper-Conference.pdf

[8] Yiting Cheng, Fangyun Wei, Jianmin Bao, Dong Chen, and Wenqiang Zhang. 2023. Adpl: Adaptive dual path learning for domain adaptation of semantic segmentation. *IEEE Transactions on Pattern Analysis and Machine Intelligence* (2023).

[9] Christoph Feichtenhofer, Haoqi Fan, Jitendra Malik, and Kaiming He. 2019. Slowfast networks for video recognition. In *Proceedings of the IEEE/CVF international conference on computer vision*. 6202–6211.

[10] S Alireza Golestaneh, Saba Dadsetan, and Kris M Kitani. 2022. No-reference image quality assessment via transformers, relative ranking, and self-consistency. In *Proceedings of the IEEE/CVF winter conference on applications of computer vision*. 1220–1230.

[11] Ian J Goodfellow, Jonathon Shlens, and Christian Szegedy. 2014. Explaining and harnessing adversarial examples. *arXiv preprint arXiv:1412.6572* (2014).

[12] Chuan Guo, Mayank Rana, Moustapha Cisse, and Laurens van der Maaten. 2018. Countering Adversarial Images using Input Transformations. In *International Conference on Learning Representations*.

[13] Kaiming He, Xiangyu Zhang, Shaoqing Ren, and Jian Sun. 2016. Deep residual learning for image recognition. In *Proceedings of the IEEE conference on computer vision and pattern recognition*. 770–778.

[14] Martin Heusel, Hubert Ramsauer, Thomas Unterthiner, Bernhard Nessler, and Sepp Hochreiter. 2017. Gans trained by a two time-scale update rule converge to a local nash equilibrium. *Advances in neural information processing systems* 30 (2017).

[15] Hossein Hosseini and Radha Poovendran. 2018. Semantic Adversarial Examples. In *Proceedings of the IEEE Conference on Computer Vision and Pattern Recognition (CVPR) Workshops*.

[16] Ziqi Huang, Yinan He, Jiashuo Yu, Fan Zhang, Chenyang Si, Yuming Jiang, Yuanhan Zhang, Tianxing Wu, Qingyang Jin, Nattapol Chanpaisit, et al. 2023. Vbench: Comprehensive benchmark suite for video generative models. *arXiv preprint arXiv:2311.17982* (2023).

[17] Cassidy Laidlaw and Soheil Feizi. 2019. Functional Adversarial Attacks. In *Advances in Neural Information Processing Systems*, H. Wallach, H. Larochelle, A. Beygelzimer, F. d'Alché-Buc, E. Fox, and R. Garnett (Eds.), Vol. 32. Curran Associates, Inc. https://proceedings.neurips.cc/paper_files/paper/2019/file/6e923226e43cd6fac7cfe1e13ad000ac-Paper.pdf

[18] Fangzhou Liao, Ming Liang, Yinpeng Dong, Tianyu Pang, Xiaolin Hu, and Jun Zhu. 2018. Defense against adversarial attacks using high-level representation guided denoiser. In *Proceedings of the IEEE conference on computer vision and pattern recognition*. 1778–1787.

[19] Ze Liu, Jia Ning, Yue Cao, Yixuan Wei, Zheng Zhang, Stephen Lin, and Han Hu. 2022. Video swin transformer. In *Proceedings of the IEEE/CVF conference on computer vision and pattern recognition*. 3202–3211.

[20] Ilya Loshchilov and Frank Hutter. 2017. Decoupled weight decay regularization. *arXiv preprint arXiv:1711.05101* (2017).

[21] Yiqiang Lv, Jingjing Chen, Zhipeng Wei, Kai Chen, Zuxuan Wu, and Yu-Gang Jiang. 2023. Downstream Task-agnostic Transferable Attacks on Language-Image Pre-training Models. In *2023 IEEE International Conference on Multimedia and Expo (ICME)*. IEEE, 2831–2836.

[22] Chenlin Meng, Yutong He, Yang Song, Jiaming Song, Jiajun Wu, Jun-Yan Zhu, and Stefano Ermon. 2021. Sdedit: Guided image synthesis and editing with stochastic differential equations. *arXiv preprint arXiv:2108.01073* (2021).

[23] Ron Mokady, Amir Hertz, Kfir Aberman, Yael Pritch, and Daniel Cohen-Or. 2023. Null-text inversion for editing real images using guided diffusion models. In *Proceedings of the IEEE/CVF Conference on Computer Vision and Pattern Recognition*. 6038–6047.

[24] Daniel Neimark, Omri Bar, Maya Zohar, and Dotan Asselmann. 2021. Video transformer network. In *Proceedings of the IEEE/CVF international conference on computer vision*. 3163–3172.

[25] Weili Nie, Brandon Guo, Yujia Huang, Chaowei Xiao, Arash Vahdat, and Anima Anandkumar. 2022. Diffusion models for adversarial purification. *arXiv preprint arXiv:2205.07460* (2022).

[26] Mandela Patrick, Dylan Campbell, Yuki Asano, Ishan Misra, Florian Metze, Christoph Feichtenhofer, Andrea Vedaldi, and Joao F Henriques. 2021. Keeping your eye on the ball: Trajectory attention in video transformers. *Advances in neural information processing systems* 34 (2021), 12493–12506.

[27] Alec Radford, Jong Wook Kim, Chris Hallacy, Aditya Ramesh, Gabriel Goh, Sandhini Agarwal, Girish Sastry, Amanda Askell, Pamela Mishkin, Jack Clark, et al. 2021. Learning transferable visual models from natural language supervision. In *International conference on machine learning*. PMLR, 8748–8763.

[28] Robin Rombach, Andreas Blattmann, Dominik Lorenz, Patrick Esser, and Björn Ommer. 2022. High-resolution image synthesis with latent diffusion models. In *Proceedings of the IEEE/CVF conference on computer vision and pattern recognition*. 10684–10695.

[29] Ali Shahin Shamsabadi, Ricardo Sanchez-Matilla, and Andrea Cavallaro. 2020. ColorFool: Semantic Adversarial Colorization. In *Proceedings of the IEEE/CVF Conference on Computer Vision and Pattern Recognition (CVPR)*.

[30] Mahmood Sharif, Sruti Bhagavatula, Lujo Bauer, and Michael K Reiter. 2016. Accessorize to a crime: Real and stealthy attacks on state-of-the-art face recognition. In *Proceedings of the 2016 acm sigsac conference on computer and communications security*. 1528–1540.

[31] Shaolin Su, Qingsen Yan, Yu Zhu, Cheng Zhang, Xin Ge, Jinqiu Sun, and Yanning Zhang. 2020. Blindly assess image quality in the wild guided by a self-adaptive hyper network. In *Proceedings of the IEEE/CVF conference on computer vision and pattern recognition*. 3667–3676.

[32] Hossein Talebi and Peyman Milanfar. 2018. NIMA: Neural image assessment. *IEEE transactions on image processing* 27, 8 (2018), 3998–4011.

[33] Du Tran, Heng Wang, Lorenzo Torresani, Jamie Ray, Yann LeCun, and Manohar Paluri. 2018. A closer look at spatiotemporal convolutions for action recognition. In *Proceedings of the IEEE conference on Computer Vision and Pattern Recognition*. 6450–6459.

[34] Ruikui Wang, Yuanfang Guo, and Yunhong Wang. 2023. Global-local characteristic excited cross-modal attacks from images to videos. In *Proceedings of the AAAI Conference on Artificial Intelligence*, Vol. 37. 2635–2643.

[35] Xin Wang, Jie Ren, Shuyun Lin, Xiangming Zhu, Yisen Wang, and Quanshi Zhang. 2020. A unified approach to interpreting and boosting adversarial transferability. *arXiv preprint arXiv:2010.04055* (2020).

[36] Zhipeng Wei, Jingjing Chen, Micah Goldblum, Zuxuan Wu, Tom Goldstein, and Yu-Gang Jiang. 2022. Towards transferable adversarial attacks on vision transformers. In *Proceedings of the AAAI Conference on Artificial Intelligence*, Vol. 36. 2668–2676.

[37] Zhipeng Wei, Jingjing Chen, Zuxuan Wu, and Yu-Gang Jiang. 2022. Boosting the transferability of video adversarial examples via temporal translation. In *Proceedings of the AAAI Conference on Artificial Intelligence*, Vol. 36. 2659–2667.

[38] Zhipeng Wei, Jingjing Chen, Zuxuan Wu, and Yu-Gang Jiang. 2022. Cross-modal transferable adversarial attacks from images to videos. In *Proceedings of the IEEE/CVF conference on computer vision and pattern recognition*. 15064–15073.

[39] Zhipeng Wei, Jingjing Chen, Zuxuan Wu, and Yu-Gang Jiang. 2023. Enhancing the self-universality for transferable targeted attacks. In *Proceedings of the IEEE/CVF conference on computer vision and pattern recognition*. 12281–12290.

[40] Cihang Xie, Jianyu Wang, Zhishuai Zhang, Zhou Ren, and Alan Yuille. 2017. Mitigating adversarial effects through randomization. *arXiv preprint arXiv:1711.01991* (2017).

[41] Weilin Xu, David Evans, and Yanjun Qi. 2017. Feature squeezing: Detecting adversarial examples in deep neural networks. *arXiv preprint arXiv:1704.01155* (2017).

[42] Ceyuan Yang, Yinghao Xu, Jianping Shi, Bo Dai, and Bolei Zhou. 2020. Temporal pyramid network for action recognition. In *Proceedings of the IEEE/CVF conference on computer vision and pattern recognition*. 591–600.

[43] Shengming Yuan, Qilong Zhang, Lianli Gao, Yaya Cheng, and Jingkuan Song. 2022. Natural Color Fool: Towards Boosting Black-box Unrestricted Attacks. In *Advances in Neural Information Processing Systems*, S. Koyejo, S. Mohamed, A. Agarwal, D. Belgrave, K. Cho, and A. Oh (Eds.), Vol. 35. Curran Associates, Inc., 7546–7560. https://proceedings.neurips.cc/paper_files/paper/2022/file/31d0d59fe946684bb228e9c8e887e176-Paper-Conference.pdf

[44] Richard Zhang, Phillip Isola, Alexei A Efros, Eli Shechtman, and Oliver Wang. 2018. The unreasonable effectiveness of deep features as a perceptual metric. In *Proceedings of the IEEE conference on computer vision and pattern recognition*. 586–595.

[45] Zhengyu Zhao, Zhuoran Liu, and Martha Larson. 2020. Adversarial color enhancement: Generating unrestricted adversarial images by optimizing a color filter. *arXiv preprint arXiv:2002.01008* (2020).

[46] Zhengyu Zhao, Zhuoran Liu, and Martha Larson. 2020. Towards large yet imperceptible adversarial image perturbations with perceptual color distance. In *Proceedings of the IEEE/CVF conference on computer vision and pattern recognition*. 1039–1048.